

# Asymmetric magnetic reconnection with a flow shear and applications to the magnetopause

C. E. Doss<sup>1</sup>, C. M. Komar<sup>1,a</sup>, P. A. Cassak<sup>1</sup>, F. D. Wilder<sup>2</sup>, S. Eriksson<sup>2</sup>, and  
J. F. Drake<sup>3</sup>

---

P. A. Cassak, Department of Physics and Astronomy, White Hall, Box 6315, West Virginia University, Morgantown, WV 26506. (Paul.Cassak@mail.wvu.edu)

<sup>1</sup>Department of Physics and Astronomy,  
West Virginia University, Morgantown,  
West Virginia, USA

<sup>2</sup>Laboratory of Atmospheric and Space  
Physics, University of Colorado, Boulder,  
Colorado, USA

<sup>3</sup>Institute for Research in Electrons and  
Applied Physics, University of Maryland,  
College Park, Maryland, USA

arXiv:1509.01575v1 [physics.space-ph] 4 Sep 2015

**Abstract.** We perform a systematic theoretical and numerical study of anti-parallel two-dimensional magnetic reconnection with asymmetries in the plasma density and reconnecting magnetic field strength in addition to a bulk flow shear across the reconnection site in the plane of the reconnecting fields, which commonly occurs at planetary magnetospheres. We analytically predict the speed at which an isolated X-line is convected by the flow, the reconnection rate, and the critical flow speed at which reconnection no longer takes place for arbitrary reconnecting magnetic field strengths, densities, and upstream flow speeds, and we confirm the results with two-fluid numerical simulations. The predictions and simulation results counter the prevailing model of reconnection at Earth's dayside magnetopause which says reconnection occurs with a stationary X-line for sub-Alfvénic magnetosheath flow, reconnection occurs but the X-line convects for magnetosheath flows between the Alfvén speed and double the Alfvén speed, and reconnection does not occur for magnetosheath flows greater than double the Alfvén speed. In particular, we find that X-line motion is governed by momentum conservation from the upstream flows, which are weighted differently in asymmetric systems, so the X-line convects for generic conditions including sub-Alfvénic upstream speeds. For the reconnection rate, as with symmetric reconnection, it drops with increasing flow shear and there is a cutoff speed above which reconnection is not predominant. However, while the cutoff condition for symmetric reconnection is that the difference in flows on the two sides of the reconnection site is twice the Alfvén speed, we find asymmetries cause the cut-

off speed for asymmetric reconnection to be higher than twice the asymmetric form of the Alfvén speed. The stronger the asymmetries, the more the cutoff exceeds double the asymmetric Alfvén speed. This is due to the fact that in asymmetric reconnection, the plasma with the smaller mass flux into the dissipation region contributes a smaller mass to the dissipation region, so the effect of its flow on opposing the release of energy by the reconnected magnetic fields is diminished and the reconnection is not suppressed to the extent previously thought. The results compare favorably with an observation of reconnection at Earth's polar cusps during a period of northward interplanetary magnetic field, where reconnection occurs despite the magnetosheath flow speed being more than twice the magnetosheath Alfvén speed, the previously proposed suppression condition. These results are expected to be of broad importance for magnetospheric physics of Earth and other planets; particular applications are discussed.

## 1. Introduction

A key element controlling the interaction of the solar wind with Earth’s magnetosphere is the nature and efficiency of the magnetic reconnection process at the dayside magnetopause. During reconnection, solar wind magnetic field lines effectively break and cross-connect with terrestrial magnetic field lines. As a consequence, solar wind plasma is able to enter the magnetosphere and the reconnected magnetic field lines convect tailward [Dungey, 1961]. This is a crucial aspect of space weather phenomena. The focus of this study is how the bulk flow of the solar wind around the magnetosphere itself affects the dayside reconnection process; we focus on (1) the convection of the reconnection site by the bulk flow, (2) the effect on the reconnection rate, and (3) the critical bulk flow speed above which reconnection is not the dominant effect.

Bulk flow is expected to be most important when reconnection occurs near the polar cusps. This is because the bulk magnetosheath flow around the magnetopause acquires a potentially sizable component parallel or anti-parallel to the magnetic field when the reconnection site is near the cusps. This affects the reconnection site very differently than when reconnection is near the subsolar point, where the flow is predominantly not aligned with the reconnecting magnetosheath magnetic field. As pointed out by Dungey [1963], magnetic reconnection is likely to occur near the polar cusps when the interplanetary magnetic field (IMF) has a northward component. Detections of high latitude reconnection are quite common [Gosling *et al.*, 1986, 1991, 1996; Kessel *et al.*, 1996; Fuselier *et al.*, 2000a; Onsager *et al.*, 2001; Avakov *et al.*, 2001; Federov *et al.*, 2001; Phan *et al.*, 2001; Frey *et al.*, 2003; Phan *et al.*, 2003; Lavraud *et al.*, 2004, 2005; Retinó *et al.*, 2005; Retinó *et al.*,

2006; *Phan et al.*, 2006, 2007; *Hasegawa et al.*, 2008; *Fuselier et al.*, 2010, 2012, 2014a; *Muzamil et al.*, 2014; *Wilder et al.*, 2014].

One reason the effect of the solar wind flow on reconnection is interesting is that there have been conflicting results on whether the cusp reconnection site is stationary or is convected tailward. *Cowley and Owen* [1989] and *Gosling et al.* [1991] suggested that in order to see sunward flow from a reconnection event poleward of the cusp with a stationary X-line (where the reconnecting magnetic field goes to zero), the magnetosheath flow speed should be sub-Alfvénic; if the flow is super-Alfvénic, the X-line would have to convect tailward. If the magnetosheath flow is more than double the magnetosheath Alfvén speed, reconnection could not occur. Tailward convection of an X-line has been seen in global magnetospheric simulations using magnetohydrodynamic simulations of Earth [*Berchem et al.*, 1995] and hybrid (kinetic ions with fluid electrons) simulations of Mercury [*Omidi et al.*, 2006]. In the latter, once the X-line convected far enough tailward, a new X-line formed. This behavior was identified in Cluster observations [*Hasegawa et al.*, 2008]. In other studies, the stability of auroral signals associated with high-latitude reconnection suggest reconnection sites remain stationary [*Fuselier et al.*, 2000a; *Frey et al.*, 2003], although there are uncertainties about whether a lack of change in auroral signatures necessarily precludes repeated X-line generation and tailward convection. It was also suggested that reconnection with magnetosheath flow speed exceeding twice the magnetosheath Alfvén speed can occur because suppressing reconnection would introduce a pileup of magnetic flux that creates plasma depletion layers, which increase the local Alfvén speed [*Fuselier et al.*, 2000b].

Another reason this topic is interesting is that a flow shear, such as that caused by the solar wind, slows down the reconnection process and can even stop it. It has been shown analytically and numerically using the magnetohydrodynamic (MHD) model for symmetric systems (with equal and opposite reconnecting magnetic fields and the same mass density on either side of the reconnection site) that a super-Alfvénic flow shear completely suppresses reconnection, while reconnection still occurs for sub-Alfvénic flow shear [Mitchell Jr. and Kan, 1978; Chen and Morrison, 1990; La Belle-Hamer et al., 1994]. When reconnection occurs with a sub-Alfvénic flow shear present, there is a decrease in the reconnection rate [Chen et al., 1997; Li and Ma, 2010; Faganello et al., 2010; Cassak and Otto, 2011; Voslion et al., 2011; Zhang et al., 2011; Wu et al., 2013] and outflow speed [Cassak, 2011]. The situation is more complicated in more realistic models than MHD; there are regimes in the Hall-MHD model in which both tearing (the linear form of reconnection) and Kelvin-Helmholtz can be simultaneously linearly unstable [Chacón et al., 2003].

The suppression of reconnection by a flow shear is potentially of broader importance. It was suggested that suppression of reconnection by flow shear limits the length of the X-line (*i.e.*, the separator) at the dayside [Borovsky et al., 2013; Borovsky, 2013]. However, Komar et al. [2015] pointed out reconnection suppression via flow shear is not expected to play a role for southward IMF orientations because the bulk flow is oriented out of the reconnection plane (along the flanks) rather than parallel to the reconnecting magnetic field (toward the poles), although it does locally decrease the reconnection rate when the IMF is directed northward.

The effect of flow shear on reconnection is also expected to be relevant at other planets. Earth's solar wind-magnetospheric interaction is qualitatively different from Jupiter's and Saturn's, where the planet's relatively rapid rotation contributes to the global convection pattern [Vasyliunas, 1983]. Studies have investigated the extent that reconnection occurs at the outer planets' magnetopauses and whether flow shear plays a role in preventing it [Masters *et al.*, 2012; Desroche *et al.*, 2012, 2013; Masters, 2014; Fuselier *et al.*, 2014b]. The solar wind-magnetospheric interaction at Mercury is similar to Earth's but on a much more rapid time scale [Slavin *et al.*, 2009], so flow shear may also affect reconnection at Mercury.

For applications at Earth's magnetosphere, it is important to note that the magnetospheric magnetic field is typically a few times stronger than the magnetosheath magnetic field and the solar wind plasma in the magnetosheath typically has a much higher density than that of the magnetosphere [Phan and Paschmann, 1996; Ku and Sibeck, 1997], *i.e.*, the reconnection is asymmetric. Consequently, it is crucial to extend studies of flow shear to asymmetric systems. There has been much work of late on asymmetric reconnection in the absence of flow shear; we summarize only those results most germane to the present study. The rate of two-dimensional (2D) asymmetric reconnection (with anti-parallel magnetic fields) has been studied [Borovsky and Hesse, 2007; Cassak and Shay, 2007]; it will be summarized in Sec. 2. In addition, it was found that the X-line and the stagnation point, where the inflowing plasma bulk flow speed goes to zero, are generally not in the same location for asymmetric reconnection [Priest *et al.*, 2000; Siscoe *et al.*, 2002; Dorelli *et al.*, 2004; Cassak and Shay, 2007].

We know of only a few numerical studies of the impact of flow shear on asymmetric magnetic reconnection. *La Belle-Hamer et al.* [1995] studied reconnection with an asymmetric density and a flow shear in fluid simulations; they suggested that reconnection is suppressed if the flow shear exceeds the Alfvén speed on either side of the layer. *Tanaka et al.* [2010] used kinetic particle-in-cell simulations to study reconnection with a density asymmetry, a flow shear, and a guide field; they observed that the X-line convects in the outflow direction with contributions from both the flow shear and the diamagnetic drift [*Swisdak et al.*, 2003].

In the present study, we use theoretical and numerical techniques to study asymmetric reconnection with arbitrary upstream parallel flow speeds. We predict the bulk convection speed of an isolated X-line using a simple fluid analysis. An interesting conclusion is that the asymmetries introduce qualitative differences compared to symmetric reconnection. In particular, if the upstream flow is equal and opposite on the two sides, the X-line is stationary for symmetric reconnection but convects for asymmetric reconnection. We also predict the reconnection rate of asymmetric reconnection with upstream flow, including a condition for the critical upstream flow speed required to suppress reconnection. The critical flow shear (half the difference of the flows on either side) for symmetric reconnection is the Alfvén speed, so one might expect the cutoff for asymmetric reconnection to be the asymmetric generalization of the Alfvén speed. However, we show that the cutoff exceeds the asymmetric Alfvén speed, and the cutoff speed becomes much larger than the asymmetric Alfvén speed when the asymmetry is large, such as the typical conditions at Earth’s magnetopause. Consequently, an isolated X-line at Earth’s polar cusps would almost never be suppressed by flow shear. We use 2D two-fluid simulations to confirm the

predictions. (We point out that particle-in-cell simulations are ostensibly a better tool to test the theory because of their more accurate description of kinetic scale physics and plasma mixing in collisionless plasmas, but fluid simulations are employed here as a first step because they accurately portray the large scale physics while being less noisy and therefore easier to compare to the new theory presented here. We employ this approach because it has proven prudent for asymmetric reconnection without flow shear [*Cassak and Shay*, 2007, 2008, 2009; *Malakit et al.*, 2010]. Important features which are present in particle-in-cell simulations but not two-fluid simulations are discussed in detail in the conclusion section.) We then show that the predictions are consistent with recent observations of a cusp reconnection event for which the magnetosheath flow exceeded twice the magnetosheath Alfvén speed. The present results are in stark contrast to the previous understanding of the effect of flow shear on reconnection based on the *Cowley and Owen* [1989] results, as X-lines convect even for sub-Alfvénic flow and reconnection occurs for magnetosheath flow speeds much greater than the magnetosheath Alfvén speed.

The layout of this paper is as follows: Section 2 has the derivation of an expression for the convection speed of the X-line and a prediction for the reconnection rate for asymmetric reconnection with a flow shear. Section 3 reviews the numerical techniques and parameters for the simulations. Section 4 presents the results of our simulations. Section 5 discusses implications for observations and applications to planetary magnetospheres. Section 6 summarizes the results and discusses limitations of the study.

## 2. Theory

We begin by defining system variables for asymmetric reconnection with upstream flow parallel or anti-parallel to the reconnecting magnetic fields. The upstream magnetic fields

above and below the dissipation region are  $\mathbf{B}_1$  and  $\mathbf{B}_2$ , which are assumed anti-parallel (*i.e.*, there is no guide field). The magnetic fields are in opposite directions, so we will use  $B_1$  and  $B_2$  as the magnitudes of the fields. (Their direction does not impact the present analysis as long as they are oppositely directed.) The upstream mass densities are  $\rho_1$  and  $\rho_2$ , and the density in the downstream region is  $\rho_{\text{out}}$ .

The upstream flow speeds  $v_{L,1}$  and  $v_{L,2}$  are defined in a stationary frame (with the planet in question at rest or, in the case of a simulation, the rest frame of the simulation), where  $L$  refers to the reconnecting magnetic field direction (as in boundary normal coordinates). Each speed is defined as positive if to the right and negative if to the left. The convection speed of the X-line is defined as  $v_{\text{drift}}$ . The inflow speeds (normal to the dissipation region) are  $v_{in,1}$  and  $v_{in,2}$ , and  $L_d$  and  $\delta$  are the half-length and half-width of the dissipation region, respectively.

It is convenient to analyze this system in the rest frame of the X-line, so we transform into the reference frame moving at a speed  $v_{\text{drift}}$  relative to the stationary reference frame. The dissipation region in this reference frame is sketched in Fig. 1. In this frame, the upstream parallel flow speeds are given by  $v_{L,1} - v_{\text{drift}}$  and  $v_{L,2} - v_{\text{drift}}$ . The outflow speed is  $v_{\text{out}}$ , which is expected to be the same in both outflow directions in the rest frame of the X-line. We define  $x$  to be the direction of the outflow ( $L$  in boundary normal coordinates). A number of potentially important effects are ignored to keep the analysis tractable; these are discussed in Sec. 6.

### 2.1. Prediction of the X-line Convection Speed

We first consider the convection of an isolated X-line for 2D anti-parallel asymmetric reconnection with arbitrary upstream parallel flow speeds. The physical reason that the

X-line can convect in the outflow direction is that the upstream plasmas carry momentum in the outflow direction; by conservation of momentum, if the upstream plasma has a non-zero net momentum, then the dissipation region will too. This is true both for symmetric and asymmetric reconnection. For symmetric reconnection, the X-line is expected to convect at the average of the upstream flows. For asymmetric reconnection, the inflow speed is different for the two upstream sides when the system has asymmetric magnetic field strengths [Cassak and Shay, 2007], so the two upstream plasmas do not contribute momentum in the outflow direction equally. Consequently, as we will show, the X-line convects in the outflow direction for asymmetric reconnection even for equal and opposite upstream flow speeds. An alternate, but equivalent, interpretation is that the X-line and stagnation point are separated during asymmetric reconnection [Cassak and Shay, 2007], so the side with the plasma that crosses the X-line imposes a flow in the outflow direction at the X-line, causing it to convect.

To estimate the convection speed, we use a fluid description of the plasma to find the bulk effects of the flow. The governing equation is the momentum equation of MHD, which in conservative form is

$$\frac{\partial(\rho\mathbf{v})}{\partial t} + \nabla \cdot \left[ \rho\mathbf{v}\mathbf{v} + \left( P + \frac{B^2}{8\pi} \right) \mathbf{I} - \frac{\mathbf{B}\mathbf{B}}{4\pi} \right] = 0, \quad (1)$$

where  $\rho$  is the plasma density,  $\mathbf{v}$  is the bulk velocity,  $P$  is the gas pressure,  $\mathbf{B}$  is the magnetic field, and  $\mathbf{I}$  is the unit tensor. Take the volume integral of Eq. (1) over the entire dissipation region. For steady-state reconnection, the time derivative term vanishes. From the divergence theorem, the remaining term becomes

$$\oint d\mathbf{S} \cdot \left[ \rho\mathbf{v}\mathbf{v} + \left( P + \frac{B^2}{8\pi} \right) \mathbf{I} - \frac{\mathbf{B}\mathbf{B}}{4\pi} \right] = 0, \quad (2)$$

where  $d\mathbf{S}$  is a differential area element directed normal to the boundary of the dissipation region. For both the upstream and downstream boundaries, the magnetic field is approximately parallel to the boundaries, so the  $\mathbf{B}\mathbf{B}$  term does not contribute. Total pressure is balanced across the dissipation region, so the pressure term has no net contribution. The  $x$  component of the surviving term of Eq. (2) is

$$\oint d\mathbf{S} \cdot (\rho\mathbf{v}v_x) = 0. \quad (3)$$

Performing a scaling analysis on this gives

$$2L_d\rho_1[v_{in,1}(v_{L,1} - v_{\text{drift}})] + 2L_d\rho_2[v_{in,2}(v_{L,2} - v_{\text{drift}})] \sim 0, \quad (4)$$

where the two terms are the contributions from the two upstream sides and the  $x$  directed momentum flux on the downstream edges cancel. Conservation of magnetic flux implies  $v_{in,1}B_1 \sim v_{in,2}B_2$  [Cassak and Shay, 2007], so solving for  $v_{\text{drift}}$  gives

$$v_{\text{drift}} \sim \frac{\rho_1 B_2 v_{L,1} + \rho_2 B_1 v_{L,2}}{\rho_1 B_2 + \rho_2 B_1}. \quad (5)$$

This gives the convection speed of the X-line in the outflow direction for arbitrary upstream densities, reconnecting magnetic field strengths, and parallel flow speeds. As discussed earlier,  $v_{\text{drift}}$  is non-zero for symmetric anti-parallel flow ( $v_{L,1} = -v_{L,2}$ ) when the magnetic fields and/or densities are asymmetric. This shows that the X-line convects regardless of upstream flow speeds, not only for super Alfvénic flow as suggested in Cowley and Owen [1989].

We consider particular limits of this expression. For any upstream conditions, if  $v_{L,1} = v_{L,2} \equiv v_{\text{shear}}$ , then  $v_{\text{drift}} = v_{\text{shear}}$ , as expected. For the case of symmetric reconnection with  $B_1 = B_2$  and  $\rho_1 = \rho_2$ , Eq. (5) reduces to the expected result of

$$v_{\text{drift}} \sim \frac{v_{L,1} + v_{L,2}}{2}, \quad (6)$$

the average of the two upstream flow velocities (which is zero if the flows are equal and opposite). If the densities are symmetric but the magnetic fields are not, then

$$v_{\text{drift}} \sim \frac{B_2 v_{L,1} + B_1 v_{L,2}}{B_2 + B_1} \quad (7)$$

and if the magnetic fields are symmetric but densities are not, we find

$$v_{\text{drift}} \sim \frac{\rho_1 v_{L,1} + \rho_2 v_{L,2}}{\rho_1 + \rho_2}. \quad (8)$$

These predictions are testable with simulations.

## 2.2. Prediction of the Reconnection Rate

We turn to the prediction of the reconnection rate of 2D asymmetric anti-parallel reconnection with arbitrary upstream parallel flow speeds. The reconnection rate  $E_{\text{shear,sym}}$  for symmetric reconnection with an equal and opposite upstream flow was recently found to scale as [Cassak and Otto, 2011]

$$E_{\text{shear,sym}} \sim E_0 \left( 1 - \frac{v_{\text{shear}}^2}{c_A^2} \right), \quad (9)$$

where  $E_0$  is the reconnection rate in the absence of upstream flow ( $\simeq 0.1$  for collisionless reconnection),  $v_{\text{shear}}$  is the upstream speed of the symmetric plasma bulk flow, and  $c_A$  is the outflow speed given by the Alfvén speed based on the reconnecting magnetic field. Physically, the form of this correction is motivated in a way similar to the suppression of reconnection by diamagnetic effects. Swisdak *et al.* [2010] argued that the magnetic tension force on the plasma due to a newly reconnected magnetic field line has to overcome the momentum of the moving plasma in the dissipation region.

For asymmetric reconnection, we propose that the effect is very similar. One main difference is that the outflow speed during 2D anti-parallel asymmetric reconnection becomes

[*Cassak and Shay, 2007; Swisdak and Drake, 2007*]

$$c_{A,\text{asym}}^2 \sim \frac{B_1 B_2}{4\pi} \frac{B_1 + B_2}{\rho_1 B_2 + \rho_2 B_1}. \quad (10)$$

A second difference is that the X-line and stagnation point are not at the center of the dissipation region [*Cassak and Shay, 2007*], so the upstream plasmas on the two sides contribute momentum in proportion to the relative location of the stagnation point. This is illustrated in Fig. 2, showing a recently reconnected magnetic field line in blue with the stagnation point denoted by the ‘‘S’’. The distance from the upstream edges to the stagnation point above and below are  $\delta_{S1}$  and  $\delta_{S2}$ , and the left side shows how the two upstream flows impact the straightening magnetic field line. Thus, not only is the upstream momentum allowed to be different on the two sides because the density and flow speed can differ, but they contribute in different proportions to the dissipation region.

We follow the result of Eq. (A3) from *Swisdak et al. [2010]* and propose the outflow speed decreases as

$$v_{\text{out}}^2 \sim c_{A,\text{asym}}^2 - \frac{\delta_{S1}}{2\delta} (v_{L,1} - v_{\text{drift}})^2 - \frac{\delta_{S2}}{2\delta} (v_{L,2} - v_{\text{drift}})^2. \quad (11)$$

In writing this, we effectively subtract off the energy due to the flow, but here we do so in proportion to each side’s contribution opposing the release of magnetic energy. Using  $\delta_{S1}/2\delta = \rho_1 B_2 / (\rho_1 B_2 + \rho_2 B_1)$  and  $\delta_{S2}/2\delta = \rho_2 B_1 / (\rho_1 B_2 + \rho_2 B_1)$  [*Cassak and Shay, 2007*] and eliminating  $v_{\text{drift}}$  using Eq. (5), some algebra reveals

$$v_{\text{out}}^2 \sim c_{A,\text{asym}}^2 - (v_{L,1} - v_{L,2})^2 \frac{\rho_1 B_2 \rho_2 B_1}{(\rho_1 B_2 + \rho_2 B_1)^2}. \quad (12)$$

Note, the only upstream flow dependence is on the difference in upstream flows  $v_{L,1} - v_{L,2}$ .

Consequently, we suggest the reconnection rate  $E_{\text{shear,asym}}$  for asymmetric reconnection with arbitrary upstream parallel flow speeds, extending Eq. (9) to asymmetric systems,

scales as

$$E_{\text{shear,asym}} \sim E_{0,\text{asym}} \left( 1 - \frac{v_{\text{shear}}^2}{c_{A,\text{asym}}^2} \frac{4\rho_1 B_2 \rho_2 B_1}{(\rho_1 B_2 + \rho_2 B_1)^2} \right), \quad (13)$$

where

$$E_{0,\text{asym}} \sim \frac{B_1 B_2}{B_1 + B_2} \frac{c_{A,\text{asym}}}{c} \frac{2\delta}{L_d} \quad (14)$$

is the asymmetric reconnection rate in the absence of upstream flow [*Cassak and Shay, 2007*] and

$$v_{\text{shear}} = \frac{v_{L,1} - v_{L,2}}{2} \quad (15)$$

is half the difference of the upstream flow speeds (their average if oppositely directed).

Thus, the reconnection rate decreases with increasing flow shear.

An important consequence of Eq. (13) is the prediction of a critical flow speed  $v_{\text{shear,crit}}$  above which reconnection does not occur (corresponding to  $E_{\text{shear,asym}} = 0$ ). The prediction is that reconnection shuts off above flow shear speeds of

$$v_{\text{shear,crit}} \sim c_{A,\text{asym}} \frac{\rho_1 B_2 + \rho_2 B_1}{2(\rho_1 B_2 \rho_2 B_1)^{1/2}}. \quad (16)$$

In the symmetric reconnection limit, this expression reduces to  $v_{\text{shear,crit}} \sim c_A$ , the known result, so it generalizes the known result to asymmetric systems. It is important to note that the fraction multiplying  $c_{A,\text{asym}}$  is always greater than or equal to one. This implies that the critical flow shear required to suppress asymmetric reconnection exceeds the asymmetric Alfvén speed. For larger asymmetries, the critical flow shear becomes larger. Consequently, while super-Alfvénic flow is sufficient to suppress symmetric reconnection, reconnection can proceed in asymmetric reconnection for super-Alfvénic flow, which differs from the *Cowley and Owen* [1989] prediction. If the asymmetry is large (as

is typical at Earth’s magnetopause), then the suppression condition is much larger than the asymmetric Alfvén speed. This is discussed further in Sec. 5.

### 3. Simulation Setup

To test the predictions, we perform 2D simulations using the massively parallel two-fluid code F3D [Shay *et al.*, 2004]. The code solves for the density, ion velocity, magnetic field, and ion pressure (assumed to be an adiabatic ideal gas with ratio of specific heats  $\gamma = 5/3$ ). Electrons are assumed cold for simplicity. The numerical algorithm is the trapezoidal leapfrog in time and fourth order finite difference in space.

The code evolves variables normalized to  $B_0$ , the reference magnetic field strength, and  $\rho_0$ , the reference mass density, where these quantities typically are the initial values on one upstream side of the simulation. Other variable’s normalizations are derived from these values: velocities are normalized to the Alfvén speed  $c_{A0} = B_0/(4\pi\rho_0)^{1/2}$ , lengths are normalized to the ion inertial length  $d_{i0} = (m_i c^2/4\pi n_0 e^2)^{1/2}$ , times are normalized to the inverse ion cyclotron frequency  $\Omega_{ci}^{-1} = (eB_0/m_i c)^{-1}$ , electric fields are normalized to  $c_{A0} B_0/c$ , and pressures are normalized to  $B_0^2/4\pi$ , where  $m_i$  and  $e$  are the ion mass and charge and  $n_0 = \rho_0/m_i$  is the plasma number density. The  $x, y$  and  $z$  directions are aligned with the initial direction of the magnetic field ( $L$  in boundary normal coordinates), the inflow ( $N$ ), and the out-of-plane current ( $M$ ).

Periodic boundary conditions are used in each direction. The size of the computational domain is  $L_x \times L_y = 204.8 \times 102.4 d_{i0}$ , and the grid scale is  $0.05 d_{i0}$  in each direction. The electron mass is  $m_e = m_i/25$ , and it is not expected that the large-scale behavior seen in our simulations is sensitive to this value.

The initial conditions for the simulation have a magnetic field profile given by an asymmetric double Harris sheet,

$$B_x(y) = \begin{cases} -B_{01} \tanh\left(\frac{|y|-L_y/4}{w_0}\right) & L_y/4 < |y| < L_y/2 \\ -B_{02} \tanh\left(\frac{|y|-L_y/4}{w_0}\right) & 0 < |y| < L_y/4 \end{cases} \quad (17)$$

with an initial current sheet width of  $w_0 = d_{i0}$ . We do not use an initial out-of-plane (guide) magnetic field. The initial density profile is

$$\rho(y) = \frac{\rho_{01} + \rho_{02}}{2} - \frac{\rho_{01} - \rho_{02}}{2} \tanh\left(\frac{|y| - L_y/4}{w_0}\right), \quad (18)$$

with asymptotic values  $\rho_{01}$  in the central portion of the domain and  $\rho_{02}$  at the top and bottom of the domain. The initial pressure profile is chosen to balance the pressure identically, with a minimum value of  $\beta_{\min} B_{\max}^2 / 8\pi$ , where  $B_{\max} = \max(B_{01}, B_{02})$  is the stronger of the two magnetic field strengths and  $\beta_{\min}$  is the minimum plasma beta on either side of the plasma. We choose  $\beta_{\min} = 2$ .

The bulk flow is initialized with a profile of

$$v_x(y) = \begin{cases} -v_1 \tanh\left(\frac{|y|-L_y/4}{w_0}\right) & L_y/4 < |y| < L_y/2 \\ -v_2 \tanh\left(\frac{|y|-L_y/4}{w_0}\right) & 0 < |y| < L_y/4. \end{cases} \quad (19)$$

We use the same  $w_0$  as for the magnetic field profile (although this is not a requirement [Li and Ma, 2010]). The upstream flow speeds are  $v_1$  and  $v_2$ , which for the simulations presented here, are always equal and opposite:  $v_1 = -v_2$ . We define this common speed as  $v_{\text{shear}}$ , which points to the left at the top and bottom of the computational domain and to the right in the central part of the domain.

The simulations do not employ any explicit resistivity or viscosity. However, there is a fourth order diffusion used in each evolution equation to damp noise at the grid scale, with coefficient  $1 \times 10^{-4}$  for asymmetric magnetic field simulations and  $1.25 \times 10^{-5}$  for asymmetric density simulations. The magnetic field is perturbed initially with random

noise of amplitude  $0.00005 B_0$  to break symmetry, which allows any secondary magnetic islands that arise to be ejected. A coherent magnetic perturbation of the form  $\delta\mathbf{B} = -(0.012B_0L_y/2\pi)\hat{\mathbf{z}} \times \nabla[\sin(2\pi x/L_x)\sin^2(2\pi y/L_y)]$  is used to initiate reconnection in a controllable manner.

A series of numerical simulations is performed with initial magnetic asymmetries of 3 or 2 with uniform density and with plasma density asymmetries of 3 with symmetric magnetic field. The initial flow speed  $v_{\text{shear}}$  in the upstream regions is varied between 0 and  $2.4 c_{A0}$ . Table 1 shows a list of the various simulations from which data are collected.

#### 4. Results

We begin with a case study showing that the X-line in asymmetric reconnection convects in the outflow direction for equal and opposite upstream flow speeds. The simulation has asymmetric magnetic fields  $B_1 = 3 B_0$  and  $B_2 = B_0$  and symmetric density  $\rho_1 = \rho_2 = \rho_0$  with an upstream flow speed of  $v_{\text{shear}} = 1.2 c_{A0}$ . Figure 3 shows the out-of-plane current density  $J_z$  as the background, with magnetic field lines overplotted in blue for a portion of the computational domain. The top, middle, and lower panels are at times  $t = 90, 105,$  and  $120 \Omega_{ci}^{-1}$ , respectively. The X-line, located near the peak in the current density, clearly convects to the right as shown by the white arrow. It travels approximately  $18 d_{i0}$  in  $30 \Omega_{ci}^{-1}$ , giving a convection speed close to  $0.6 c_{A0}$ , which is the predicted speed from Eq. (5).

To extract more quantitative information from the simulations, the systems are evolved until a steady-state is reached with the X-line convection speeds and reconnection rates being relatively constant. To apply a common criterion for the steady-state across simulations (which have different reconnection rates), we put a condition on the size of the primary magnetic islands; all simulations presented here are relatively steady when the

island half widths are between 7 and 11  $d_{i0}$ . X-line convection speeds and reconnection rates are measured during these times.

The X-line and O-line are found in the standard way as the saddle point and local extremum, respectively, near the current sheets of the flux function  $\psi$  given by  $\mathbf{B} = \hat{\mathbf{z}} \times \nabla \psi$ . The X-line convection speed is obtained from the time average of the time derivative of the position of the X-line during the steady-state interval. The reconnection rate is the average of the time rate of change of the difference in magnetic flux between the X-line and the O-line.

#### 4.1. The X-line Convection Speed

For the X-line convection speed, we first use simulations with asymmetric magnetic fields, symmetric plasma densities, and symmetric upstream flow. The  $x$  coordinate of the X-line in the simulation reference frame is plotted as a function of time in Fig. 4. The (blue) solid line is from a simulation with  $B_1 = 3 B_0, B_2 = B_0$  and the (red) dashed line is for  $B_1 = 2 B_0, B_2 = B_0$ , both with  $v_{\text{shear}} = 1.2 c_{A0}$ . The convection speed is higher with the stronger magnetic field, as predicted, with measured values of  $v_{\text{drift}} = 0.63 c_{A0}$  for  $B_1 = 3 B_0$  and  $0.37 c_{A0}$  for  $B_1 = 2 B_0$ , compared to predicted values from Eq. (7) of 0.60 and  $0.40 c_{A0}$ .

To test the upstream flow speed dependence, Fig. 5 shows the average drift speed  $v_{\text{drift}}$  as a function of upstream flow speed  $v_{\text{shear}}$  for simulations with  $B_1 = 3 B_0$  and  $B_2 = B_0$ . Here, and throughout, the (blue) triangles are for the top current sheet and the (red) squares are for the bottom current sheet. The prediction from Eq. (7) is plotted as the dashed line, and the results clearly agree well with the prediction.

Simulations with symmetric magnetic fields but with asymmetric plasma densities were also carried out. However, we do not expect the numerical results to be reliable because of a known problem with the fluid approach in systems with asymmetric density. In particular, fluid simulations require conduction to allow for plasma mixing [Cassak and Shay, 2009]; newly reconnected field lines have different densities and temperatures, and in the absence of conduction the strong parallel temperature gradient persists instead of the plasmas mixing. These simulations do not contain conduction and it is unlikely the standard fluid closure reproduces the more realistic kinetic mixing in a collisionless dissipation region. Particle-in-cell simulations will be required to assess this prediction for asymmetric densities.

## 4.2. The Reconnection Rate

For the reconnection rate in systems with asymmetries and upstream flow, we plot the reconnection rate  $E$  as a function of flow speed  $v_{\text{shear}}$  in Fig. 6(a) for simulations with fixed  $B_1 = 3 B_0$  and  $B_2 = B_0$  for upstream flow speeds from 0 to  $1.6 c_{A0}$ . The prediction from Eq. (13) is plotted as the dashed line, where  $E_{0,\text{asym}}$  is chosen as the measured value of the reconnection rate in the simulation with no upstream flow. The agreement is very good. The result for  $v_{\text{shear}} = 1.2 c_{A0}$  falls a little below the curve; this simulation had a significant secondary island unlike the others which motivates its slightly worse performance.

A similar study is carried out with simulations of asymmetric plasma densities but with symmetric magnetic field. While the convection speed is not expected to be correct in these simulations, it was argued that the reconnection rate is reliable [Cassak and Shay, 2009; Birn et al., 2010]. (This is because redoing the calculation of the outflow speed

and reconnection rate from *Cassak and Shay* [2007] for a system where the downstream plasma does not mix leads to the same expressions as for the system where mixing occurs. The differences arise only in the sub-structure of the dissipation region.) The results for a simulation study with  $\rho_1 = \rho_0$  and  $\rho_2 = 3 \rho_0$  with upstream flow speeds varied from 0 to  $0.6 c_{A0}$  are shown in Fig. 6(b). The prediction from Eq. (13) is plotted as the dashed line. For asymmetric densities, the agreement with the prediction is again very good.

### 4.3. The Cessation Condition

We now test the condition for the cessation of reconnection, given by Eq. (16). For the series of simulations with  $B_1 = 3 B_0, B_2 = B_0, \rho_1 = \rho_2 = \rho_0$ , we have  $c_{A,\text{asym}} = \sqrt{3} c_{A0}$  from Eq. (10), so  $v_{\text{shear,crit}} = 2 c_{A0}$ . In the simulations, we see that reconnection occurs, with the predicted reconnection rate and X-line drift speed, for  $v_{\text{shear}} = 1.6 c_{A0}$ . In contrast, for  $v_{\text{shear}} = 2.4 c_{A0}$ , there is a phase change and reconnection is not the dominant effect. This is shown in Fig. 7, which gives the out-of-plane current density  $J_z$  for this simulation. There is clear evidence of the early phases of a Kelvin-Helmholtz instability. We note that reconnection is known to occur as a secondary instability of Kelvin-Helmholtz in a plasma, and that does occur here, but this is fundamentally different than the reconnection-dominated current sheets displayed in Fig. 3. We note that for  $v_{\text{shear}} = 2 c_{A0}$ , right at the predicted cutoff, there is a hybrid of reconnection and Kelvin-Helmholtz rolls forming. Thus, the results are consistent with the prediction. As the qualitative behavior near the cutoff becomes more challenging to assess, it is prohibitive to pin down the transition flow speed to higher precision than done here.

The asymmetric density simulations with  $B_1 = B_2 = B_0, \rho_1 = \rho_0$ , and  $\rho_2 = 3 \rho_0$  give another opportunity to test the prediction. Here,  $c_{A,\text{asym}} = \sqrt{1/2} c_{A0}$ , so  $v_{\text{shear,crit}} =$

$\sqrt{2/3} c_{A0} \simeq 0.82 c_{A0}$ . In the simulations, reconnection does occur for  $v_{\text{shear}} = 0.6 c_{A0}$  but is not appreciable for  $v_{\text{shear}} = 0.8 c_{A0}$ , which is consistent with the predictions.

In summary, the predictions for  $v_{\text{drift}}$  in Eq. (5),  $E_{\text{shear,asym}}$  in Eq. (13), and  $v_{\text{shear,crit}}$  in Eq. (16) agree with the simulation results.

## 5. Applications to Planetary Magnetospheres

For a sample application, we consider reconnection at the cusps of Earth’s magnetosphere. We emphasize that the predictions in Sec. 2 assume an isolated X-line; we first discuss how the present results suggest isolated X-lines would act in the magnetosphere. We call side 1 “ms” for magnetosphere and side 2 “sh” for magnetosheath. For typical conditions at the magnetopause,  $\rho_{sh} \gg \rho_{ms}$  and  $B_{ms} \gtrsim B_{sh}$ . Also, the upstream flow speed in the magnetosphere  $v_{L,ms}$  is negligible, while the magnetosheath flow  $v_{L,sh}$  is due to the solar wind flowing around the magnetopause. In this limit, the X-line convection speed from Eq. (5) becomes

$$v_{\text{drift}} \simeq v_{L,sh}. \quad (20)$$

Thus, an isolated X-line would convect tailward at essentially the same speed as the flow in the magnetosheath, not the average flow speed as one would expect for symmetric reconnection. The physical cause for this, as sketched in Fig. 2, is that the stagnation point is far to the magnetospheric side of the dissipation region, so most of the dissipation region is populated by magnetosheath plasma and most of its momentum is contained in the magnetosheath plasma. Therefore, it flows near the speed of the magnetosheath plasma.

This is borne out in recent Cluster observations of a tailward convecting X-line [*Wilder et al.*, 2014] which we use as a case study. In this event at the southern hemisphere’s cusp

on December 27th, 2005, Cluster’s C1 and C3 spacecraft witnessed reconnection signatures on a crossing from the magnetosheath to the magnetosphere. The magnetosheath had  $B_{sh} \simeq 10 - 15$  nT and a number density  $n_{sh} \simeq 60 - 70$  cm<sup>-3</sup>, while in the magnetosphere  $B_{ms} \simeq 60$  nT and  $n_{ms} = 0.5$  cm<sup>-3</sup>. From their separation and the time delay between observed jet reversals, the convection speed of the X-line was estimated to be  $v_{\text{drift}} = 105$  km/s, while the  $L$  component of the magnetosheath flow was estimated at  $v_{L,sh} = 106$  km/s. This is consistent with Eq. (20).

In the past, assessing whether reconnection could occur was done by comparing the magnetosheath flow speed to the magnetosheath Alfvén speed [Cowley and Owen, 1989]. For this event, the magnetosheath Alfvén speed is 28 km/s, while the magnetosheath flow speed is 105 km/s. This exceeds twice the magnetosheath Alfvén speed so previous models would suggest reconnection should not occur, but reconnection is observed to happen. The asymmetric Alfvén speed for these parameters is 74.5 km/s, so  $v_{\text{shear}} = v_{L,sh}/2 \simeq 53$  km/s is sub-Alfvénic, and the prediction here is that reconnection should occur.

For the reconnection rate, in the limit appropriate for typical conditions at the magnetopause, Eq. (13) becomes

$$E_{\text{shear,asym}} \sim E_{0,\text{asym}} \left( 1 - \frac{4v_{\text{shear}}^2 \rho_{ms} B_{sh}}{c_{A,\text{asym}}^2 \rho_{sh} B_{ms}} \right). \quad (21)$$

Since  $\rho_{sh} \gg \rho_{ms}$ , this implies the surprising result that the reconnection rate is not changed much by the flow shear for typical magnetospheric parameters. This is a major departure from the symmetric case where the reconnection rate falls strongly as a function of flow shear speed. Physically, the cause for this is related to the stagnation point being very close to the magnetospheric side, as before. In the reference frame of the X-line, the magnetosheath is essentially still, while the magnetosphere has a significant flow. However,

since the magnetospheric density is so low, it has very little effect on the reconnection process.

This is seen further by investigating the condition for suppressing reconnection. From Eq. (21) and using  $v_{\text{shear}} \simeq v_{L,sh}/2$  from Eq. (15) since the magnetospheric plasma is essentially stationary, the condition that reconnection is suppressed ( $E_{\text{shear,asym}} \leq 0$ ) is

$$v_{L,sh} \geq c_{A,\text{asym}} \left( \frac{\rho_{sh} B_{ms}}{\rho_{ms} B_{sh}} \right)^{1/2}. \quad (22)$$

For the example of the case study event from Cluster, this implies it would take a magnetosheath flow speed of 22 times bigger than  $c_{A,\text{asym}} \simeq [B_{sh}(B_{ms} + B_{sh})/4\pi\rho_{sh}]^{1/2}$  for flow shear to suppress reconnection, far greater than in symmetric reconnection and the *Cowley and Owen* [1989] model where Alfvénic flow suppresses reconnection. (We point out further that particle-in-cell simulations and observations typically find outflow speeds half of that predicted in symmetric or asymmetric reconnection theories, so the critical speed may be a factor of two smaller than this prediction. However, this does not change the result that the critical speed is much higher than the asymmetric Alfvén speed and the magnetosheath Alfvén speed.) Thus, for an isolated X-line with typical magnetospheric parameters, the flow shear would rarely prevent reconnection from occurring.

While X-lines in the magnetosphere can convect as discussed earlier, it was suggested from observations [*Fuselier et al.*, 2000a; *Frey et al.*, 2003] that cusp reconnection can be steady for hours with a stationary X-line, though it may be difficult to be sure solely from auroral signatures. Further, the distance to the X-line has been inferred from observations [*Petrinec et al.*, 2003; *Trattner et al.*, 2007a, b], and strong convection is not seen, even though Eq. (20) would predict a large enough convection speed to be observable. This suggests that reconnection in the magnetosphere is not always consistent with isolated

X-lines, which was a key assumption of the theory presented here. In particular, the theory does not take any external effect other than flow into account. A single dayside X-line is not isolated; instead, for a single X-line during steady times to be stationary, it must balance all magnetic forces, gas pressure forces, and dynamic pressure forces from bulk flow (of the type discussed here). Thus, by definition, the flow effects have already been taken into account to set up a single X-line, and the present model would not apply. Physically, the present model does not include magnetic fields in the cusp being line-tied to the ionosphere, which is an additional force that can slow or prevent X-line convection and would undoubtedly modify the present results. It is possible that the tailward moving X-lines seen in observations [*Hasegawa et al.*, 2008; *Wilder et al.*, 2014] are related to a secondary island moving tailward; a secondary X-line is not in the same equilibrium as a single X-line, so it can convect tailward. Future work is necessary to determine the conditions under which some X-lines convect and others do not, the speed at which they convect, and their signatures in the cusp.

A second point worth making is that the results in this section would change in the presence of a high-density plasmaspheric drainage plume [*Borovsky and Steinberg*, 2006; *Borovsky and Denton*, 2006] on the magnetospheric side of the dissipation region. This increases the local density, which decreases the outflow speed [*Walsh et al.*, 2014a, b]. Plumes are most commonly observed centered around 13.6 h magnetic local time [*Walsh et al.*, 2013]. If the magnetospheric density is comparable or larger than the magnetosheath, the X-line would not convect with the magnetosheath flow, and the full expressions from Sec. 2 would be needed.

We note in passing that the significant departures between symmetric and asymmetric reconnection with a flow shear suggest that the effect of flow shear at Jupiter, Saturn, and Uranus should be revisited. The previous work on this subject employed the predictions for symmetric reconnection, so the results are likely to change with the asymmetric reconnection results presented here.

It is worth putting the present results in context of a leading model for what allows cusp reconnection to occur despite nominally super-Alfvénic flow. It was argued that the draped magnetic field during northward IMF compresses, and therefore increases, the magnetopause magnetic field, which itself causes the mass density to decrease, forming a density depletion layer at the magnetopause [*Petrinec et al.*, 2003]. Both the increased field and decreased density increase the local Alfvén speed, potentially making the flow sub-Alfvénic. The present theory *should not* be interpreted as implying that a density depletion layer does not occur or that the layer would not change the local Alfvén speed. Using the *Wilder et al.* [2014] parameters, *Petrinec et al.* [2003] would suggest (assuming that the Alfvén Mach number is based on magnetosheath parameters) that a density depletion by a factor of about 2.5 would be sufficient to make the flow sub-Alfvénic (see their Fig. 7). When based on the asymmetric Alfvén speed, the necessary depletion factor reduces to approximately 1.3. Clearly, more research is needed to identify the level of plasma depletion, its effect on cusp reconnection, and the extent to which the present results apply to the dayside magnetopause.

## 6. Discussion

In this study, we use a scaling argument based on conservation of momentum to find the convection (drift) speed of the X-line in anti-parallel 2D asymmetric magnetic reconnection.

tion with arbitrary upstream parallel flow speeds [Eq. (5)]. We also present a prediction for the reconnection rate for arbitrary upstream flow speeds [Eq. (13)]. The predictions are confirmed using 2D two-fluid numerical simulations. For asymmetric magnetic fields, the results agree well for both predictions. For asymmetric densities, simulations agree with the reconnection rate prediction, but the drift speed cannot be assessed because the fluid model does not correctly model plasma mixing. In particular, the results show that the X-line convects even for sub-Alfvénic flow, which contrasts the leading model by *Cowley and Owen* [1989].

The reconnection rate prediction gives a threshold flow shear above which reconnection does not occur [Eq. (16)], and this prediction is consistent with the simulations. This result shows that asymmetric reconnection can persist with flow shear exceeding the asymmetric Alfvén speed, and can occur even with much larger flow shear speeds if the asymmetries are large. We note that the critical speed prediction in Eq. (16) differs from the condition given by *La Belle-Hamer et al.* [1995], who suggested the critical speed is the larger of the two Alfvén speeds on either upstream side of the dissipation region. It also differs from the prediction that reconnection does not occur if the difference between the magnetosheath and magnetospheric flow exceeds twice the magnetosheath Alfvén speed [*Cowley and Owen*, 1989]. To see this, consider the simulation with  $B_1 = 3, B_2 = 1$ , a uniform density of  $\rho_1 = \rho_2 = 1$ , and a flow of  $v_{\text{shear}} = 1.6$ . Here, the magnetosheath nominally corresponds to the “2” side (with the weaker magnetic field). In the rest frame of the magnetosphere (the “1” side), the magnetosheath flow speed is 3.2. This exceeds double the magnetosheath Alfvén speed of 1. The fact that reconnection is observed in this simulation is evidence against the *Cowley and Owen* [1989] model. The fact that we do

not see reconnection in the  $v_{\text{shear}} = 2.4$  simulation is evidence against the *La Belle-Hamer et al.* [1995] model, which is below the magnetospheric Alfvén speed of 3.

The results have potentially important implications for reconnection at Earth’s magnetopause. For isolated X-lines, the predictions suggest that the X-line convects essentially with the magnetosheath flow as a consequence of the stagnation point being nearly all the way to the magnetospheric side of the dissipation region. The reconnection rate is affected by only a small amount, and it would take magnetosheath flow an order of magnitude faster than the asymmetric Alfvén speed to suppress reconnection. This is a major departure from the current understanding based on symmetric reconnection which claims magnetosheath flow greater than twice the Alfvén speed is sufficient to suppress reconnection. The results may differ for non-isolated X-lines, such as magnetic fields line-tied to the ionosphere during reconnection near the polar cusps. The results could also drastically alter previous estimates of how flow shear affects dayside reconnection at Jupiter, Saturn, and Uranus, so revisiting these results is important future work. Another potential application is determining whether the present results impact predictions for the speed of anti-sunward propagation of flux transfer events [*Cowley and Owen*, 1989; *Cooling et al.*, 2001].

The present analysis made a number of simplifying assumptions that should be addressed in future work. Since the analytical calculation uses the fluid picture, finite Larmor radius effects are ignored, but they may be important in the boundary layers [*Malakit et al.*, 2013; *Koga et al.*, 2014], especially for the dayside magnetopause where the density asymmetry is typically significant. The present analysis and simulations ignore asymmetries in the outflow direction [*Murphy et al.*, 2010; *Oka et al.*, 2011], which

may be important for reconnection near the polar cusps. In particular, asymmetries in the outflow direction cause the outflow speeds to be different in the two outflow directions [Murphy *et al.*, 2010], so future work is necessary to determine the effect of shear flow in such systems. The present analysis and simulations also do not include a guide field, which may be present [Muzamil *et al.*, 2014]. The guide field is important because, when coupled with a gas pressure gradient across the inflow direction at the dissipation region, it can set up diamagnetic effects which also have been shown to cause the X-line to convect in the outflow direction [Swisdak *et al.*, 2003; Beidler and Cassak, 2011], and therefore either reinforce or oppose the convection caused by flow shear [Tanaka *et al.*, 2010]. The analysis and simulations also do not include upstream flows in the out-of-plane direction [Wang *et al.*, 2012; Chen *et al.*, 2013; Wang *et al.*, 2014; Tassi *et al.*, 2014]. Also, the simulations used the fluid model, which does not self-consistently capture plasma mixing in the exhaust for systems with asymmetric density [Cassak and Shay, 2009]; this would be fixed using simulations employing the particle-in-cell technique [Roytershteyn and Daughton, 2008; Tanaka *et al.*, 2010]. Another future study should address asymmetric reconnection with a flow shear in line-tied systems relevant to polar cusp applications.

**Acknowledgments.** Support from NASA West Virginia Space Grant Consortium (CED and CMK), the West Virginia University Summer Undergraduate Research Experience (SURE) program (CED), and NSF Grant AGS-0953463 (PAC) is gratefully acknowledged. PAC acknowledges support from the International Space Science Institute in Bern, Switzerland. This research used resources of the National Energy Research Scientific Computing Center, a DOE Office of Science User Facility supported by the Office of Science of the U.S. Department of Energy under Contract No. DE-AC02-05CH11231.

The data used to produce the results of this paper are available from the authors. We thank M. T. Beidler, R. C. Fear, S. A. Fuselier, and B. M. Walsh for helpful conversations.

(a) Current address: NASA/Goddard Space Flight Center, Greenbelt, MD, USA

## References

- Avanov, L. A., V. N. Smirnov, J. H. W. Jr., S. A. Fuselier, and O. L. Vaisberg (2001), High-latitude magnetic reconnection in sub-Alfvénic flow: Interball Tail observations on May 29, 1996, *J. Geophys. Res.*, *106*, 29,491.
- Beidler, M. T., and P. A. Cassak (2011), Model for incomplete reconnection in sawtooth crashes, *Phys. Rev. Lett.*, *107*, 255002.
- Berchem, J., J. Raeder, and M. Ashour-Abdalla (1995), Magnetic flux ropes at the high-latitude magnetopause, *Geophys. Res. Lett.*, *22*, 1189.
- Birn, J., J. E. Borovsky, M. Hesse, and K. Schindler (2010), Scaling of asymmetric reconnection in compressible plasmas, *Phys. Plasmas*, *17*, 052108.
- Borovsky, J. E. (2013), Physics-based solar wind driver functions for the magnetosphere: Combining the reconnection-coupled MHD generator with the viscous interaction, *J. Geophys. Res.*, *118*, 7119.
- Borovsky, J. E., and M. H. Denton (2006), Effect of plasmaspheric drainage plumes on solar-wind/magnetosphere coupling, *Geophys. Res. Lett.*, *33*, L20101.
- Borovsky, J. E., and M. Hesse (2007), The reconnection of magnetic fields between plasmas with different densities: Scaling relations, *Phys. Plasmas*, *14*, 102309.
- Borovsky, J. E., and J. T. Steinberg (2006), The “calm before the storm” in cir/magnetosphere interactions: Occurrence statistics, solar wind statistics, and mag-

- netospheric preconditioning, *J. Geophys. Res.*, *111*, A07S10.
- Borovsky, J. E., M. H. Denton, R. E. Denton, V. K. Jordanova, and J. Krall (2013), Estimating the effects of ionospheric plasma on solar wind/magnetosphere coupling via mass loading of dayside reconnection: Ion-plasma-sheet oxygen, plasmaspheric drainage plumes, and the plasma cloak, *J. Geophys. Res.*, *118*, 5695.
- Cassak, P. A. (2011), Theory and simulations of the scaling of magnetic reconnection with symmetric shear flow, *Phys. Plasmas*, *18*, 072106.
- Cassak, P. A., and A. Otto (2011), Scaling of the reconnection rate with anti-parallel symmetric shear flow, *Phys. Plasmas*, *18*, 074501.
- Cassak, P. A., and M. A. Shay (2007), Scaling of asymmetric magnetic reconnection: General theory and collisional simulations, *Phys. Plasmas*, *14*, 102114.
- Cassak, P. A., and M. A. Shay (2008), Scaling of asymmetric Hall Reconnection, *Geophys. Res. Lett.*, *35*, L19102.
- Cassak, P. A., and M. A. Shay (2009), Structure of the dissipation region in fluid simulations of asymmetric magnetic reconnection, *Phys. Plasmas*, *16*, 055704.
- Chacón, L., D. A. Knoll, and J. M. Finn (2003), Hall MHD effects on the 2D Kelvin-Helmholtz/tearing instability, *Phys. Lett. A*, *308*, 187.
- Chen, Q., A. Otto, and L. C. Lee (1997), Tearing instability, Kelvin-Helmholtz instability, and magnetic reconnection, *J. Geophys. Res.*, *102*, 151.
- Chen, X. L., and P. J. Morrison (1990), Resistive tearing instability with equilibrium shear flow, *Phys. Fluids B*, *2*, 495.
- Chen, Y. G., C. J. Xiao, X. G. Wang, J. Q. Wang, H. Zhang, Z. Y. Pu, Z. W. Ma, and Z. B. Guo (2013), The influence of out-of-plane shear flow on Hall magnetic reconnection

- and FTE generation, *J. Geophys. Res.*, *118*, 4279.
- Cooling, B. M. A., C. J. Owen, and S. J. Schwartz (2001), Role of the magnetosheath flow in determining the motion of open flux tubes, *J. Geophys. Res.*, *106*, 18,763.
- Cowley, S. W. H. and C. J. Owen (1989), A simple illustrative model of open flux tube motion over the dayside magnetopause, *Planet. Space Sci.*, *37*, 1461.
- Desroche, M., F. Bagenal, P. A. Delamere, and N. Erkaev (2012), Conditions at the expanded Jovian magnetopause and implications for the solar wind interaction, *J. Geophys. Res.*, *117*, A07202.
- Desroche, M., F. Bagenal, P. A. Delamere, and N. Erkaev (2013), Conditions at the magnetopause of Saturn and implications for the solar wind interaction, *J. Geophys. Res.*, *118*, 3087.
- Dorelli, J. C., M. Hesse, M. M. Kuznetsova, L. Rastaetter, and J. Raeder (2004), A new look at driven magnetic reconnection at the terrestrial subsolar magnetopause, *J. Geophys. Res.*, *109*, A12216.
- Dungey, J. W. (1961), Interplanetary magnetic field and the auroral zones, *Phys. Rev. Lett.*, *6*, 47.
- Dungey, J. W. (1963), The structure of the exosphere or adventures in velocity space, in *Geophysics The Earth's Environment*, edited by C. D. Witt, J. Hieblot, and A. Lebeau, Gordon Breach, New York.
- Faganello, M., F. Pegoraro, F. Califano, and L. Marradi (2010), Collisionless magnetic reconnection in the presence of a sheared velocity field, *Phys. Plasmas*, *17*, 062102.
- Federov, A., E. Dubinin, P. Song, A. Skalsky, and E. Budnik (2001), Structure of the flank magnetopause for horizontal IMF: INTERBALL 1 observations, *J. Geophys. Res.*, *106*,

25,419.

Frey, H. U., T. D. Phan, S. A. Fuselier, and S. B. Mende (2003), Continuous magnetic reconnection at Earth's magnetopause, *Nature*, *426*, 533.

Fuselier, S. A., S. M. Petrinec, and K. J. Trattner (2000a), Stability of the high-latitude reconnection site for steady northward IMF, *Geophys. Res. Lett.*, *27*, 473.

Fuselier, S. A., K. J. Trattner, and S. M. Petrinec (2000b), Cusp observations of high- and low-latitude reconnection for northward interplanetary magnetic field, *J. Geophys. Res.*, *105*, 255.

Fuselier, S. A., S. M. Petrinec, and K. J. Trattner (2010), Antiparallel magnetic reconnection rates at the earth's magnetopause, *J. Geophys. Res.*, *115*, A10207.

Fuselier, S. A., K. J. Trattner, S. M. Petrinec, and B. Lavraud (2012), Dayside magnetic topology at the earth's magnetopause for northward IMF, *J. Geophys. Res.*, *117*, A08235.

Fuselier, S. A., S. M. Petrinec, K. J. Trattner, and B. Lavraud (2014a), Magnetic field topology for northward IMF reconnection: Ion observations, *J. Geophys. Res.*, *119*, 9051.

Fuselier, S. A., R. Frahm, W. S. Lewis, A. Masters, J. Mukherjee, S. M. Petrinec, and I. J. Sillanpaa (2014b), The location of magnetic reconnection at Saturn's magnetopause: A comparison with Earth, *J. Geophys. Res.*, *119*, 2563.

Gosling, J. T., M. F. Thomsen, and S. J. Bame (1986), Accelerated plasma flows at the near-tail magnetopause, *J. Geophys. Res.*, *91*, 3029.

Gosling, J. T., M. F. Thomsen, S. J. Bame, and R. C. Elphic (1991), Observations of reconnection of interplanetary and lobe magnetic field lines at the high-latitude mag-

- netopause, *J. Geophys. Res.*, *96*, 14,097.
- Gosling, J. T., M. F. Thomsen, G. Le, and C. T. Russell (1996), Observations of magnetic reconnection at the lobe magnetopause, *J. Geophys. Res.*, *101*, 24,765.
- Hasegawa, H., A. Retinó, A. Vaivads, Y. Khotyaintsev, R. Nakamura, T. Takada, Y. Miyashita, H. Rème, and E. A. Lucek (2008), Retreat and reformation of X-line during quasi-continuous tailward-of-the-cusp reconnection under northward IMF, *Geophys. Res. Lett.*, *35*, L15104.
- Kessel, R. L., S.-H. Chen, J. L. Green, S. F. Fung, S. A. Boardsen, L. C. Tan, T. E. Eastman, J. D. Craven, and L. A. Frank (1996), Evidence of high-latitude reconnection during northward IMF: Hawkeye observations, *Geophys. Res. Lett.*, *23*, 583.
- Koga, D., W. D. Gonzalez, F. S. Mozer, M. V. D. Silveira, and F. R. Cardoso (2014), Larmor electric field observed at the Earth's magnetopause by Polar satellite, *Phys. Plasmas*, *21*, 100701.
- Komar, C. M., R. L. Fermo, and P. A. Cassak (2015), Comparative analysis of dayside magnetic reconnection models in global magnetosphere simulations, *J. Geophys. Res.*, *120*, 276.
- Ku, H. C., and D. G. Sibeck (1997), Internal structure of flux transfer events produced by the onset of merging at a single X line, *J. Geophys. Res.*, *102*, 2243.
- La Belle-Hamer, A. L., A. Otto, and L. C. Lee (1994), Magnetic reconnection in the presence of sheared plasma flow: Intermediate shock formation, *Phys. Plasmas*, *1*, 706.
- La Belle-Hamer, A. L., A. Otto, and L. C. Lee (1995), Magnetic reconnection in the presence of sheared flow and density asymmetry: Applications to the Earth's magnetopause, *J. Geophys. Res.*, *100*, 11,875.

- Lavraud, B., T. D. Phan, M. W. Dunlop, M. G. G. T. Taylor, P. Cargill, J.-M. Bosqued, I. Dandouras, H. Rème, J.-A. Sauvaud, C. P. Escoubet, A. Balogh, and A. Fazakerley (2004), The exterior cusp and its boundary with the magnetosheath: Cluster multi-event analysis, *Ann. Geophys.*, *22*, 3039.
- Lavraud, B., A. Fedorov, E. Budnik, M. F. Thomsen, A. Grigoriev, P. J. Cargill, M. W. Dunlop, H. Rème, I. Dandouras, and A. Balogh (2005), High-altitude cusp flow dependence on IMF orientation: A 3-year Cluster statistical study, *J. Geophys. Res.*, *110*, A02209.
- Li, J. H., and Z. W. Ma (2010), Nonlinear evolution of resistive tearing mode with sub-Alfvénic shear flow, *J. Geophys. Res.*, *115*, A09216.
- Malakit, K., M. A. Shay, P. A. Cassak, and C. Bard (2010), Scaling of asymmetric magnetic reconnection: Kinetic particle-in-cell simulation, *J. Geophys. Res.*, *115*, A10223.
- Malakit, K., M. A. Shay, P. A. Cassak, and D. Ruffolo (2013), A new electric field in asymmetric magnetic reconnection, *Phys. Rev. Lett.*, *111*, 135001.
- Masters, A. (2014), Magnetic reconnection at Uranus' magnetopause, *J. Geophys. Res.*, *119*, 5520.
- Masters, A., J. P. Eastwood, M. Swisdak, M. F. Thomsen, C. T. Russell, N. Sergis, F. J. Crary, M. K. Dougherty, A. J. Coates, and S. M. Krimigis (2012), The importance of plasma  $\beta$  for magnetic reconnection at Saturn's magnetopause, *Geophys. Res. Lett.*, *39*, L08103.
- Mitchell Jr., H. G., and J. R. Kan (1978), Merging of magnetic fields with field-aligned plasma flow components, *J. Plasma Phys.*, *20*, 31.

- Murphy, N. A., C. R. Sovinec, and P. A. Cassak (2010), Magnetic reconnection with asymmetry in the outflow direction, *J. Geophys. Res.*, *115*, A09206.
- Muzamil, F. M., C. J. Farrugia, R. B. Torbert, P. R. Pritchett, F. S. Mozer, J. D. Scudder, C. T. Russell, P. E. Sandholt, W. F. Denig, and L. Wilson III (2014), Structure of a reconnection layer poleward of the cusp: Extreme density asymmetry and a guide field, *J. Geophys. Res.*, *119*, 7343.
- Oka, M., T. Phan, J. P. Eastwood, V. Angelopoulos, N. A. Murphy, M. Oieroset, Y. Miyashita, M. Fujimoto, J. McFadden, and D. Larson (2011), Magnetic reconnection X-line retreat associated with dipolarization of the Earth's magnetosphere, *Geophys. Res. Lett.*, *38*, L20105.
- Omidi, N., X. Blanco-Cano, C. T. Russell, and H. Karimabadi (2006), Global hybrid simulations of solar wind interaction with Mercury: Magnetospheric boundaries, *Adv. Space Sci.*, *38*, 632.
- Onsager, T. G., J. D. Scudder, M. Lockwood, and C. T. Russell (2001), Reconnection at the high-latitude magnetopause during northward interplanetary magnetic field conditions, *J. Geophys. Res.*, *106*, 25,467.
- Petrinec, S. M., K. J. Trattner, and S. A. Fuselier (2003), Steady reconnection during intervals of northward IMF: Implications for magnetosheath properties, *J. Geophys. Res.*, *108*, 1458.
- Phan, T., H. U. Frey, S. Frey, L. Peticolas, S. Fuselier, C. Carlson, H. Rème, J.-M. Bosqued, A. Balogh, M. Dunlop, L. Kistler, C. Mouikis, I. Dandouras, J.-A. Sauvard, S. Mende, J. McFadden, G. Parks, E. Moebius, B. Klecker, G. Paschmann, M. Fujimoto, S. Petrinec, M. F. Marcucci, A. Korth, and R. Lundin (2003), Simultaneous Cluster and

- IMAGE observations of cusp reconnection and auroral proton spot for northward IMF, *Geophys. Res. Lett.*, *30*, 1509.
- Phan, T. D., and G. Paschmann (1996), Low-latitude dayside magnetopause and boundary layer for high magnetic shear, 1: Structure and motion, *J. Geophys. Res.*, *101*, 7801.
- Phan, T. D., B. U. O. Sonnerup, and R. P. Lin (2001), Fluid and kinetics signatures of reconnection at the dawn tail magnetopause: Wind observations, *J. Geophys. Res.*, *106*, 25,489.
- Phan, T. D., J. T. Gosling, M. S. Davis, R. M. Skoug, M. Oieroset, R. P. Lin, R. P. Lepping, D. J. McComas, C. W. Smith, H. Reme, and A. Balogh (2006), A magnetic reconnection X-line extending more than 390 Earth radii in the solar wind, *Nature*, *439*, 175.
- Phan, T. D., J. F. Drake, M. A. Shay, F. S. Mozer, and J. P. Eastwood (2007), Evidence for an elongated ( $>60$  ion skin depths) electron diffusion region during fast magnetic reconnection, *Phys. Rev. Lett.*, *99*, 255002.
- Priest, E. R., V. S. Titov, R. E. Grundy, and A. W. Hood (2000), Exact solutions for reconnective magnetic annihilation, *Proc. Roy. Soc. Lon. A*, *456*, 1821.
- Retinó, A., M. B. Bavassano Cattaneo, M. F. Marcucci, A. Vaivads, M. André, Y. Khotyaintsev, T. Phan, G. Pallochia, H. Réme, E. Möbius, B. Klecker, C. W. Carlson, M. McCarthy, A. Korth, R. Lundin, and A. Balogh (2005), Cluster multi-spacecraft observations at the high-latitude duskside magnetopause: Implications for continuous and component magnetic reconnection, *Ann. Geophys.*, *23*, 461.

- Retinó, A., A. Vaivads, M. André, F. Sahraoui, Y. Khotyaintsev, J. S. Pickett, M. B. B. Cattaneo, M. F. Marcucci, M. Morooka, C. J. Owen, S. C. Buchert, and N. Comilleau-Wehrin (2006), Structure of the separatrix region close to a magnetic reconnection X-line: Cluster observations, *Geophys. Res. Lett.*, *33*, L06101.
- Roytershteyn, V., and W. Daughton (2008), Collisionless instability of thin current sheets in the presence of sheared parallel flows, *Phys. Plasmas*, *15*, 082901.
- Shay, M. A., J. F. Drake, M. Swisdak, and B. N. Rogers (2004), The scaling of embedded collisionless reconnection, *Phys. Plasmas*, *11*, 2199.
- Siscoe, G. L., G. M. Erickson, B. U. Ö. Sonnerup, N. C. Maynard, J. A. Schoendorf, K. D. Siebert, D. R. Weimer, W. W. White, and G. R. Wilson (2002), Flow-through magnetic reconnection, *Geophys. Res. Lett.*, *29*, 1626.
- Slavin, J. A., M. H. Acuña, B. J. Anderson, D. N. Baker, M. Benna, S. A. Boardsen, G. Gloeckler, R. E. Gold, G. C. Ho, H. Korth, S. M. Krimigis, and R. L. McNutt (2009), MESSENGER observations of magnetic reconnection in Mercury's magnetosphere, *Science*, *324*, 606.
- Swisdak, M., and J. F. Drake (2007), Orientation of the reconnection X-line, *Geophys. Res. Lett.*, *34*, L11106.
- Swisdak, M., J. F. Drake, M. A. Shay, and B. N. Rogers (2003), Diamagnetic suppression of component magnetic reconnection at the magnetopause, *J. Geophys. Res.*, *108*, 1218.
- Swisdak, M., M. Opher, J. F. Drake, and F. Alounai Bibi (2010), The vector direction of the interstellar magnetic field outside the heliosphere, *Ap. J.*, *710*, 1769.
- Tanaka, K. G., M. Fujimoto, and I. Shinohara (2010), Physics of magnetopause reconnection: A study of the combined effects of density asymmetry, velocity shear, and guide

- field, *Int. J. Geophys.*, 2010, 202583.
- Tassi, E., D. Grasso, and L. Comisso (2014), Linear stability analysis of collisionless reconnection in the presence of an equilibrium flow aligned with the guide field, *EPJ D.*, 68, 88.
- Trattner, K. J., J. S. Mulcock, S. M. Petrinec and S. A. Fuselier (2007a), Location of the reconnection line at the magnetopause during southward IMF conditions, *Geophys. Res. Lett.*, 34, L03108.
- Trattner, K. J., J. S. Mulcock, S. M. Petrinec and S. A. Fuselier (2007b), Probing the boundary between antiparallel and component reconnection during southward interplanetary magnetic field conditions, *J. Geophys. Res.*, 112, A08210.
- Vasyliunas, V. M. (1983), *Plasma distribution and flow*, chap. 395, edited by A. J. Dessler, Cambridge Univ. Press, Cambridge, UK.
- Voslion, T., O. Agullo, P. Beyer, M. Yagi, S. Benkadda, X. Garbet, K. Itoh, and S.-I. Itoh (2011), Impact of a shear flow on double tearing nonlinear dynamics, *Phys. Plasmas*, 18, 063302.
- Walsh, B. M., D. G. Sibeck, Y. Nishimura, and V. Angelopoulos (2013), Statistical analysis of the plasmaspheric plume at the magnetopause, *J. Geophys. Res.*, 118, 1.
- Walsh, B. M., T. D. Phan, D. G. Sibeck, and V. M. Souza (2014a), The plasmaspheric plume and magnetopause reconnection, *Geophys. Res. Lett.*, 41, 223.
- Walsh, B. M., J. C. Foster, P. J. Erickson, and D. G. Sibeck (2014b), Simultaneous ground- and space-based observations of the plasmaspheric plume and reconnection, *Science*, 343, 1122.

- Wang, J., C. Xiao, and X. Wang (2012), Effects of out-of-plane shear flows on fast reconnection in a two-dimensional hall magnetohydrodynamics model, *Phys. Plasmas*, *19*, 032905.
- Wang, L., X. Q. Wang, X. G. Wang, and Y. Liu (2014), Out-of-plane shear flow effects on fast magnetic reconnection in a two-dimensional hybrid simulation model, *Chin. Phys. B*, *23*, 025203.
- Wilder, F. D., S. Eriksson, K. J. Trattner, P. A. Cassak, S. A. Fuselier, and B. Lybekk (2014), Observation of a retreating X line and magnetic islands poleward of the cusp during northward interplanetary magnetic field conditions, *J. Geophys. Res.*, *119*, 9643.
- Wu, L. N., L. Z. Jiang, F. Y. Hong, and L. Xu (2013), The effects of a shear flow on nonlinear evolutions of double tearing mode in Hall magnetohydrodynamics, *Phys. Letters A*, *377*, 2373.
- Zhang, X., L. J. Li, L. C. Wang, J. H. Li, and Z. W. Ma (2011), Influences of sub-Alfvénic shear flows on nonlinear evolution of magnetic reconnection in compressible plasmas, *Phys. Plasmas*, *18*, 092112.

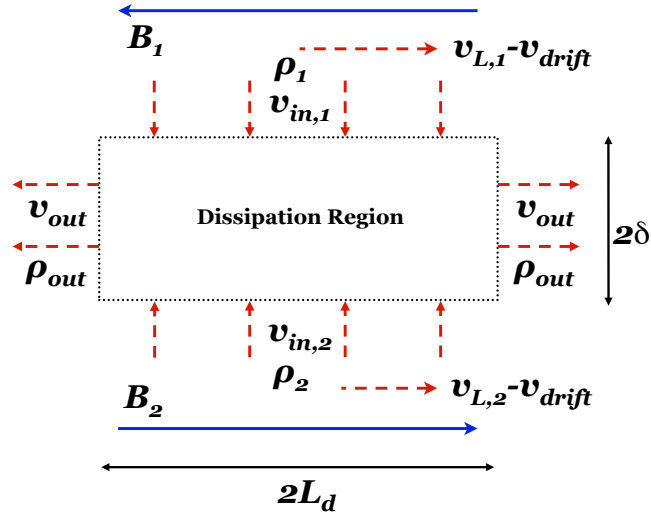


**Figure 1.** Sketch of a reconnection region for asymmetric reconnection with flow shear in the reference frame the dissipation region. Red dashed lines show components of plasma velocities and blue solid lines represent the reconnecting magnetic fields.

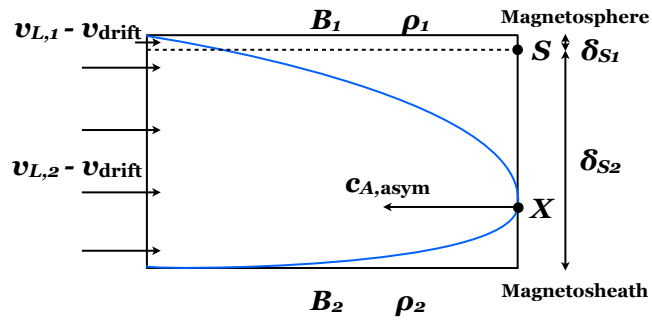


**Figure 2.** Sketch of a newly reconnected magnetic field line (blue curve) for a system with upstream flow and asymmetries. The box denotes the left half of a dissipation region. “X” and “S” mark the X-line and stagnation point, and the dashed line goes through the stagnation point. How the bulk flow impacts the dissipation region is sketched on the left side. Nominally, the relative positions of the X-line and stagnation point are representative of the magnetosphere being at the top and the magnetosheath being at the bottom.

**Table 1.** List of simulations with their initial values of upstream magnetic fields  $B_1$  and  $B_2$  (in units of  $B_0$ ), mass densities  $\rho_1$  and  $\rho_2$  (in units of  $\rho_0$ ), and upstream flow speed  $v_{\text{shear}}$  (in units of  $c_{A0}$ ). Also included is the predicted convection speed  $v_{\text{drift,pred}}$  from Eq. (5), measured convection speeds of the top ( $v_{\text{drift},T}$ ) and bottom ( $v_{\text{drift},B}$ ) current sheets, the predicted reconnection rate  $E_{\text{pred}}$  from Eq. (13) (in units of  $c_{A0}B_0/c$ ), and the measured reconnection rates from the top  $E_T$  and bottom  $E_B$  current sheets. The  $E_{0,\text{asym}}$  value is obtained from the average measured reconnection rate in runs without shear, except for the  $B_1 = 2 B_0$  simulation which uses the prediction from *Cassak and Shay* [2007] using  $\delta/L = 0.06$ .

$B_1$	$B_2$	$\rho_1$	$\rho_2$	$v_{\text{shear}}$	$v_{\text{drift,pred}}$	$v_{\text{drift},T}$	$v_{\text{drift},B}$	$E_{\text{pred}}$	$E_T$	$E_B$
3	1	1	1	0.0	0.0	0.02	-0.04	0.19	0.20	0.18
3	1	1	1	0.4	0.2	0.24	0.21	0.18	0.18	0.18
3	1	1	1	0.8	0.4	0.49	0.39	0.16	0.16	0.15
3	1	1	1	1.2	0.6	0.63	0.53	0.12	0.093	0.083
3	1	1	1	1.6	0.8	0.60	0.69	0.067	0.071	0.065
3	1	1	1	2.0	1.0	1.03	0.98	0	—	—
3	1	1	1	2.4	1.2	—	—	—	—	—
2	1	1	1	1.2	0.4	0.37	0.37	0.041	0.049	0.060
1	1	1	3	0.0	0.0	—	—	0.042	0.044	0.040
1	1	1	3	0.1	0.05	—	—	0.041	0.037	0.038
1	1	1	3	0.2	0.1	—	—	0.039	0.039	0.039
1	1	1	3	0.4	0.2	—	—	0.032	0.036	0.036
1	1	1	3	0.6	0.3	—	—	0.019	0.027	0.025
1	1	1	3	0.8	0.4	—	—	0.0017	—	—

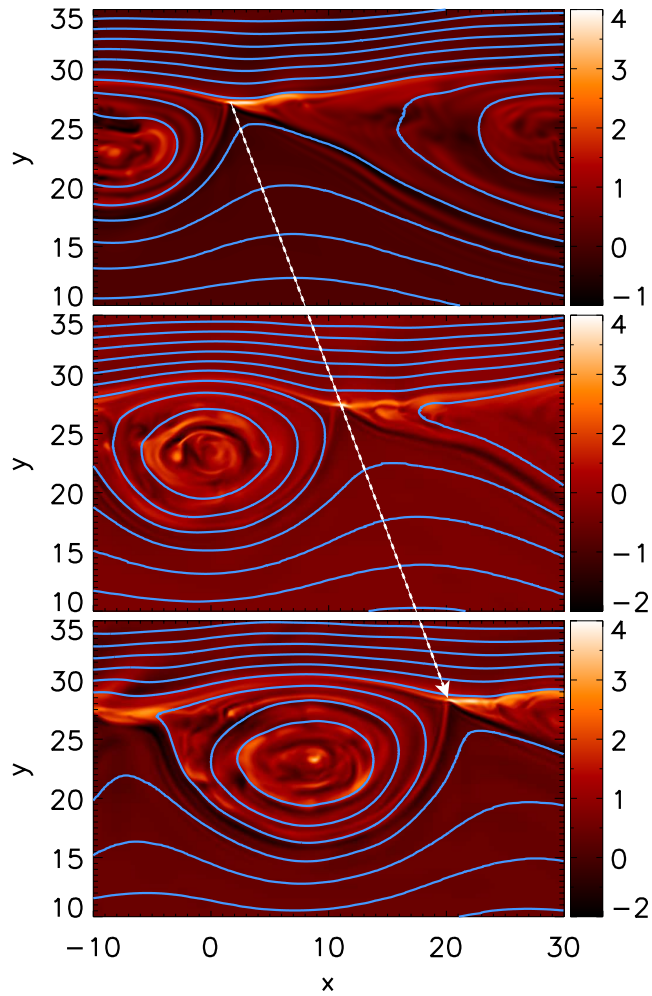


**Figure 3.** Out-of-plane current density  $J_z$  as a function of  $x$  and  $y$  (in units of  $d_{i0}$ ), with magnetic field lines overplotted in blue, for a simulation with  $v_{\text{shear}} = 1.2 c_{A0}$ ,  $B_1 = 3 B_0$ ,  $B_2 = B_0$ , and  $\rho_1 = \rho_2 = \rho_0$ . The top, middle, and bottom plots are at time  $t = 90, 105$ , and  $120 \Omega_{ci}^{-1}$ . Only a portion of the computational domain is plotted.

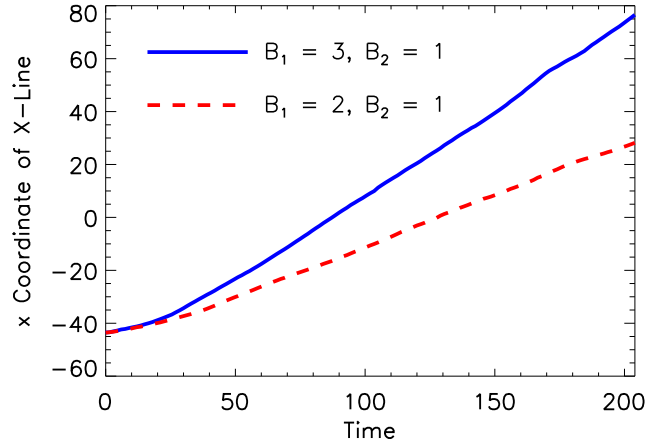


**Figure 4.** X-line position (in units of  $d_{i0}$ ) as a function of time (in units of  $\Omega_{ci}^{-1}$ ) for simulations with  $v_{\text{shear}} = 1.2 c_{A0}$  for  $B_1 = 3 B_0, B_2 = B_0$  (blue solid) and  $B_1 = 2 B_0, B_2 = B_0$  (red dashed). The average drift speeds are  $v_{\text{drift}} = 0.63 c_{A0}$  for  $B_1 = 3 B_0$  and  $v_{\text{drift}} = 0.37 c_{A0}$  for  $B_1 = 2 B_0$ .

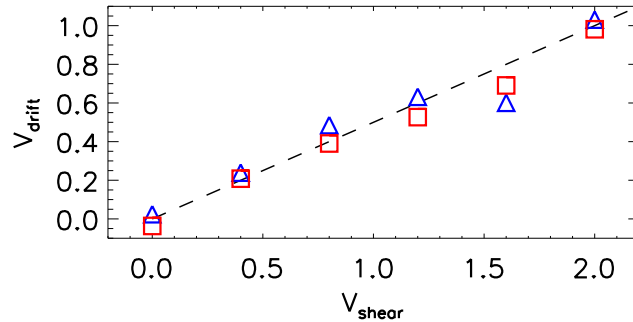


**Figure 5.** X-line convection speed  $v_{\text{drift}}$  (in units of  $c_{A0}$ ) for the top ( $\triangle$ ) and bottom ( $\square$ ) current sheets from simulations with magnetic fields  $B_1 = 3 B_0$  and  $B_2 = B_0$  as a function of upstream flow speed  $v_{\text{shear}}$  (in units of  $c_{A0}$ ). The dashed line is the prediction from Eq. (7).

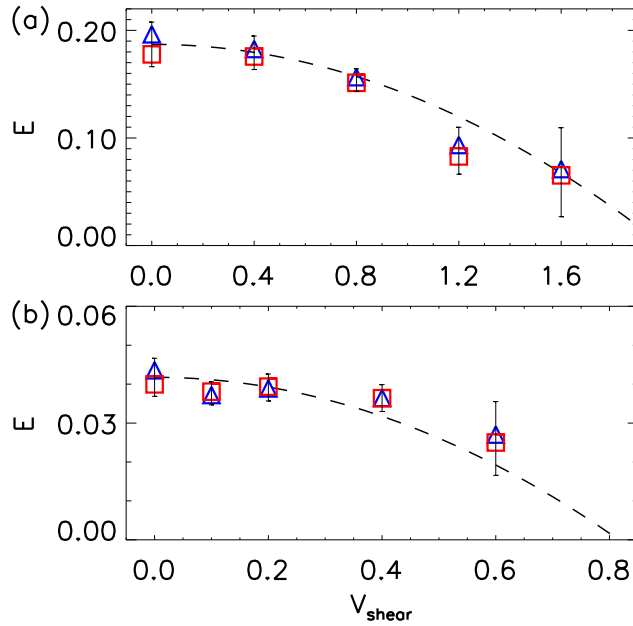


**Figure 6.** Reconnection rate  $E$  (in units of  $c_{A0}B_0/c$ ) for the top ( $\triangle$ ) and bottom ( $\square$ ) current sheets from simulations with various flow speed  $v_{\text{shear}}$  (in units of  $c_{A0}$ ) and (a) magnetic field asymmetry  $B_1 = 3 B_0$  and  $B_2 = B_0$  and (b) density asymmetry  $\rho_1 = \rho_0$  and  $\rho_2 = 3 \rho_0$ . The dashed lines are the predicted rates from Eq. (13), with  $E_{0,\text{asym}}$  as the average rate of reconnection in the absence of a sheared flow.

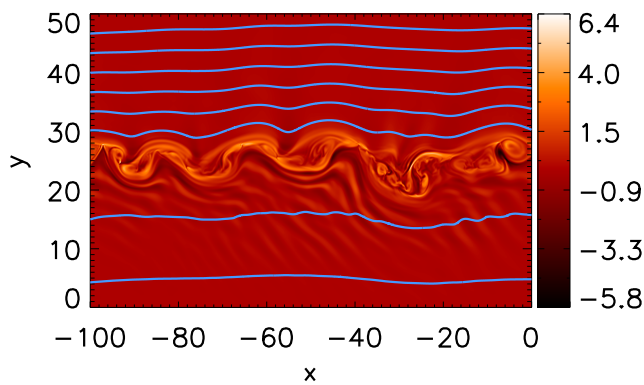


**Figure 7.** Out-of-plane current density  $J_z$ , with magnetic field lines overplotted in blue, for a simulation with  $B_1 = 3 B_0$ ,  $B_2 = B_0$ ,  $\rho_1 = \rho_2 = \rho_0$  with  $v_{\text{shear}} = 2.4 c_{A0}$ , which is above the predicted cutoff where reconnection is suppressed.